FULL PAPER

Photoswitchable Superabsorbency Based on Nanocellulose Aerogels

*Marjo Kettunen, Riitta J. Silvennoinen, Nikolay Houbenov, Antti Nykänen, Janne Ruokolainen, Jani Sainio, Viljami Pore, Marianna Kemell, Mikael Ankerfors, Tom Lindström, Mikko Ritala, Robin H. A. Ras, and Olli Ikkala**

Chemical vapor deposition of a thin titanium dioxide (TiO_2) film on lightweight native nanocellulose aerogels offers a novel type of functional material that shows photoswitching between water-superabsorbent and water-repellent states. Cellulose nanofibrils (diameters in the range of 5–20 nm) with native crystalline internal structures are topical due to their attractive mechanical properties, and they have become relevant for applications due to the recent progress in the methods of their preparation. Highly porous, nanocellulose aerogels are here first formed by freeze-drying from the corresponding aqueous gels. Well-defined, nearly conformal TiO_2 coatings with thicknesses of about 7 nm are prepared by chemical vapor deposition on the aerogel skeleton. Weighing shows that such TiO_2-coated aerogel specimens essentially do not absorb water upon immersion, which is also evidenced by a high contact angle for water of 140° on the surface. Upon UV illumination, they absorb water 16 times their own weight and show a vanishing contact angle on the surface, allowing them to be denoted as superabsorbents. Recovery of the original absorption and wetting properties occurs upon storage in the dark. That the cellulose nanofibrils spontaneously aggregate into porous sheets of different length scales during freeze-drying is relevant: in the water-repellent state they may stabilize air pockets, as evidenced by a high contact angle, in the superabsorbent state they facilitate rapid water-spreading into the aerogel cavities by capillary effects. The TiO_2-coated nanocellulose aerogels also show photo-oxidative decomposition, i.e., photocatalytic activity, which, in combination with the porous structure, is interesting for applications such as water purification. It is expected that the present dynamic, externally controlled, organic/inorganic aerogels will open technically relevant approaches for various applications.

1. Introduction

Aerogels are lightweight solid and solvent-free materials that exhibit a high porosity (typically 95%–99%) within their network structure.[1] They have been pursued for various applications due to their combination of feasible properties, such as extremely low density, low mean free path of diffusion, high specific surface area, low dielectric constant, and slow speed of sound, and they have been used as trapping media for chemical analyses.[1] A characteristic problem has been their high fragility, which has limited their use in applications where mechanical robustness is needed. To overcome this problem, aerogels based on native cellulose nanofibril networks were recently introduced, which allow suppressed brittleness and even flexibility in facile and relevant ways.[2] In this case, the long and entangled native cellulose nanofibrils form a deformable aerogel network due to their fibrillar morphology and strong mutual hydrogen bonds, and are therefore suitable for templating.[2,3] More generally, native cellulose nanofibers, i.e., long and entangled nanofibrils and rodlike nanowhiskers, are interesting materials because of their biological and sustainable

M. Kettunen,[+] R. J. Silvennoinen, Dr. N. Houbenov, A. Nykänen, Prof. J. Ruokolainen, Dr. R. H. A. Ras, Prof. O. Ikkala
Molecular Materials
Department of Applied Physics and Center for New Materials
Aalto University School of Science and Technology
(previously Helsinki University of Technology)
P.O. Box 15100, FIN-00076, Espoo, Finland
E-mail: olli.ikkala@tkk.fi

Dr. J. Sainio
The Surface Science Group
Department of Applied Physics
Aalto University School of Science and Technology
P.O. Box 11100, FIN-00076, Espoo, Finland

Dr. V. Pore, Dr. M. Kemell, Prof. M. Ritala
Laboratory of Inorganic Chemistry
Department of Chemistry
University of Helsinki
P.O. Box 55, FI-00014, Finland

M. Ankerfors, Prof. T. Lindström
Innventia AB, Process and Product Innovation
P.O. Box 5604, SE-114 86 Stockholm, Sweden

[+] Marjo Kettunen has previously published under the name Marjo Pääkkö.

DOI: 10.1002/adfm.201001431

origin.[4] Furthermore, they have a high aspect ratio, high surface area, and attractive mechanical properties.[2,5] The native cellulose nanofibers cannot be prepared by solution routes and regeneration, as the mechanically feasible cellulose I crystalline structure would be changed to an amorphous or to a cellulose II crystalline structure.[6] Also, the previous aerogels made from dissolved and regenerated cellulose suffer from the same phenomenon, which easily leads to morphological changes and increased fragility.[7,8] The liberation of the long native nanofibrils from macroscopic fibers requires specific techniques, such as mechanical shearing[9,10] or 2,2,6,6,-tetramethylpiperidine-1-oxyl (TEMPO)-mediated oxidation.[11] Recently, a mild enzymatic hydrolysis and high-pressure homogenization was introduced to liberate long and entangled 5–10 nm thick nanofibrils that form percolated networks and strong gels in water even at very low concentrations.[12,13] Subsequent freeze-drying of the networks enables aerogels with typical porosity of 98% and density of ca. 0.03 g cm^{-3}, which show deformability and robustness.[2] Importantly, the network morphology of these aerogels can be tuned from nanofibrillar to sheetlike skeletons with intrinsic micro- and nanoscale structures and porosity at several length scales by modifying the freeze-drying conditions.[2]

As the ductility and facile preparation of such nanocellulose aerogels is feasible for applications, it becomes relevant to explore functionalities upon templating. The present work introduces inorganic modification of the nanocellulose aerogel skeleton with TiO_2 using chemical vapor deposition (CVD), aiming at robust, functional, organic/inorganic hybrid aerogels. TiO_2 is a prototypic source for dynamically responsive materials:[14] for example, a flat TiO_2 surface can undergo an aqueous wetting transition from larger to lower contact angles upon UV illumination.[15] The original contact angle is recovered upon storing the sample in the dark.[15,16] Increased contact angles and even superhydrophobicity with contact angles >150° have been achieved, but this additionally requires hierarchical surface topography with combined microscale and nanoscale surface roughness.[17,18] TiO_2 is inexpensive and nontoxic and shows photocatalytic properties, stability, and biocompatibility. Studies to control the morphology of TiO_2 are abundant, since the structural properties and accessible surface area both play a significant role in the efficiency of TiO_2 in many of its applications. Previously, macroscopic cellulose fibers within wood tissue and filter papers were utilized as templates for organic–inorganic hybrids or for purely inorganic replicates of TiO_2 and several other oxides using sol–gel processes.[19–23] The macroscopic cellulose fibers of filter paper as well as peptide ribbons have also been used as a template for atomic layer deposition of TiO_2.[24,25]

Finally, superabsorbents are hydrophilic polymers capable of absorbing large quantities of water in comparison with their own weight, and they are relevant in several bulk applications.[26,27] In more specific applications, especially in biotechnology and drug-release, polymers that switch between the hydrophilic water-absorbing and hydrophobic water-repelling states are needed. A classic example is poly (*N*-isopropylacrylamide), which is temperature-switchable.[28] As inspired by the highly hydrophilic character of the nanocellulose hydrogels and aerogels, we show here that the originally superabsorbent nanocellulose aerogels are changed into water-repellent gels upon TiO_2 coating. Such TiO_2-coated aerogels further enable photoswitching of water absorption upon exposure to UV light, ranging from a very hydrophobic state to a superabsorbent, highly wetting state with a vanishing contact angle. In addition, photocatalytic properties are explored in combination with the porous aerogel structure.

2. Results and Discussion

2.1. Structure of Nanocellulose Aerogels

The structures of the macroscopic cellulose pulp fibers, aqueous cellulose nanofibrils forming the aqueous gels, and aerogels consisting of nanofibrils are illustrated in **Figure 1**. As seen in Figure 1A,B, the diameter of pulp fibers is ca. 40 µm. They are used as a starting material for the native cellulose nanofibrils. The enzymatic hydrolysis and high-pressure homogenization of pulp leads to a strong aqueous gel due to the long and mechanically entangled nature of the cellulose nanofibrils with lateral dimensions of 5–20 nm (Figure 1C, transmission electron microscopy (TEM) image), i.e., four orders of magnitude smaller than the original ones.[12,13] The aqueous gel is vacuum freeze-dried to produce aerogels (see the Experimental Section). The vacuum freeze-drying

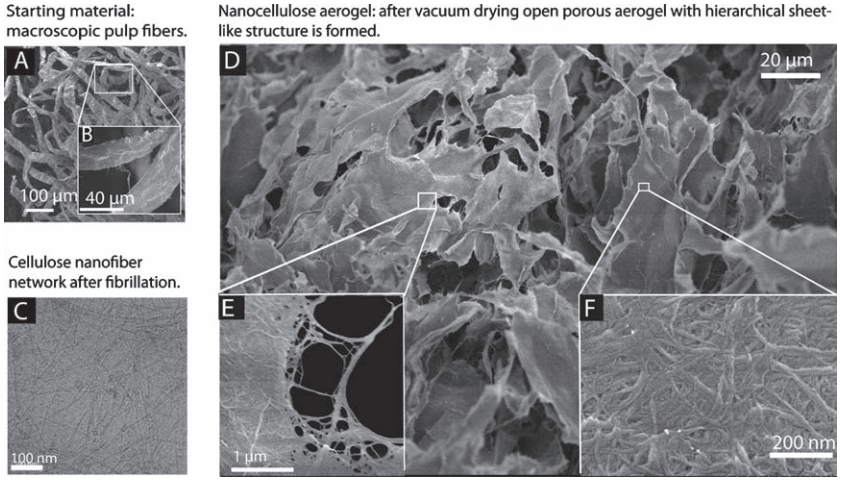

Figure 1. Electron microscopy images at different steps, from cellulose pulp via native cellulose nanofibril hydrogel to solid aerogel. FE-SEM image of macroscopic cellulose fibers in sulfite cellulose pulp (A,B). After enzymatic and mechanical treatment, a cellulose nanofibril network is formed in the aqueous medium (C; cryogenic-TEM). Most of the nanofibrils are ca. 5–20 nm in diameter. Upon vacuum freeze-drying, a sheetlike aerogel structure is formed (D; FE-SEM). The representative SEM images at high magnification show the aggregated nanofibrils, which forms nanoporosity (E) and roughness within the sheet (F).

method used in this study is a one-step process. This makes it simpler than many other freeze-drying techniques, and also simpler than supercritical CO_2 drying, which is a slow process with many steps.[7,8] It is important that the entangled cellulose nanofibrils with high aspect ratios form a strong network structure that does not collapse upon vacuum freeze-drying, but instead enables solid, foamlike, deformable white nanocellulose aerogels with a porosity of 98% and a very low density of 0.03 g cm^{-3}.[2] In this work, the hydrogels were placed in a mold and they were inserted in a vacuum oven, where the relatively slow freezing process of water leads to aggregation of the nanofibrils into 2D sheetlike structures that extend for tens of micrometers (Figure 1D). The sheets are mutually connected to form a network skeleton and between the interconnected and layered sheets there are pores of micrometer sizes and fibrous structures (Figure 1D). This is a straightforward method to achieve "overhang" or re-entrant structures at different length scales in a spontaneous manner, keeping "cavities" within the structure, which are later shown to be useful for water absorption and wetting properties. The determination of the pore size distribution of the smallest pores indicates the existence of an additional mesoporosity, i.e., pores smaller than 50 nm.[2] This suggests that the sheets, in fact, also have an internal porosity, which can be visualized in the field-emission scanning electron microscopy (FE-SEM) image in Figure 1E. Due to the large pores and extended sheetlike structure the specific Brunauer–Emmett–Teller (BET) surface area for a 3 mm thick sample is 20 m^2 g^{-1}. However, the aggregated nanofibrils (Figure 1F) generate nanoroughness within the sheets, and together with microscale sheets they impart hierarchical micro- and nanomorphology, porosity, and roughness to the aerogel.

2.2. Functionalization of Aerogels with TiO_2 by Chemical Vapor Deposition

Next, hybrid inorganic/organic aerogels were pursued based on chemical vapor deposition of a thin layer of TiO_2 on the nanocellulose aerogel substrate. In this straightforward, one-step process the nanocellulose aerogels were exposed to titanium isopropoxide vapor at 190 °C at pressures of 1–5 kPa for 2 h (see Experimental Section). The reactions of titanium isopropoxide on the nanocellulose surface can be subtle, as there are three potential reaction mechanisms: 1) reaction with the cellulose hydroxyl groups; 2) reaction with water, as there is always water absorbed on cellulose surfaces, which is difficult or even impossible to remove, suggesting that the bound water may play an important role in the CVD coating formation; 3) thermal decomposition of titanium isopropoxide.[29,30] That TiO_2 is indeed deposited is confirmed by X-ray photoelectron spectroscopy (XPS) which shows Ti 2p peaks at 458.4, 464.1, and 471.5 eV and oxygen peaks at 530 eV and around 532 eV (**Figure 2**A). The previously reported Ti $2p_{3/2}$ binding-energy ranges for different titanium oxidation states are indicated in the figure, showing that titanium is found in the +IV state.[31,32] The peak at 471.5 eV is a satellite peak related to the Ti $2p_{3/2}$ main peak of TiO_2.[32] The main oxygen peak is found at 530 eV, which is typical for TiO_2.[31] The higher energy component near 532 eV is most likely related to hydroxyl groups on the TiO_2

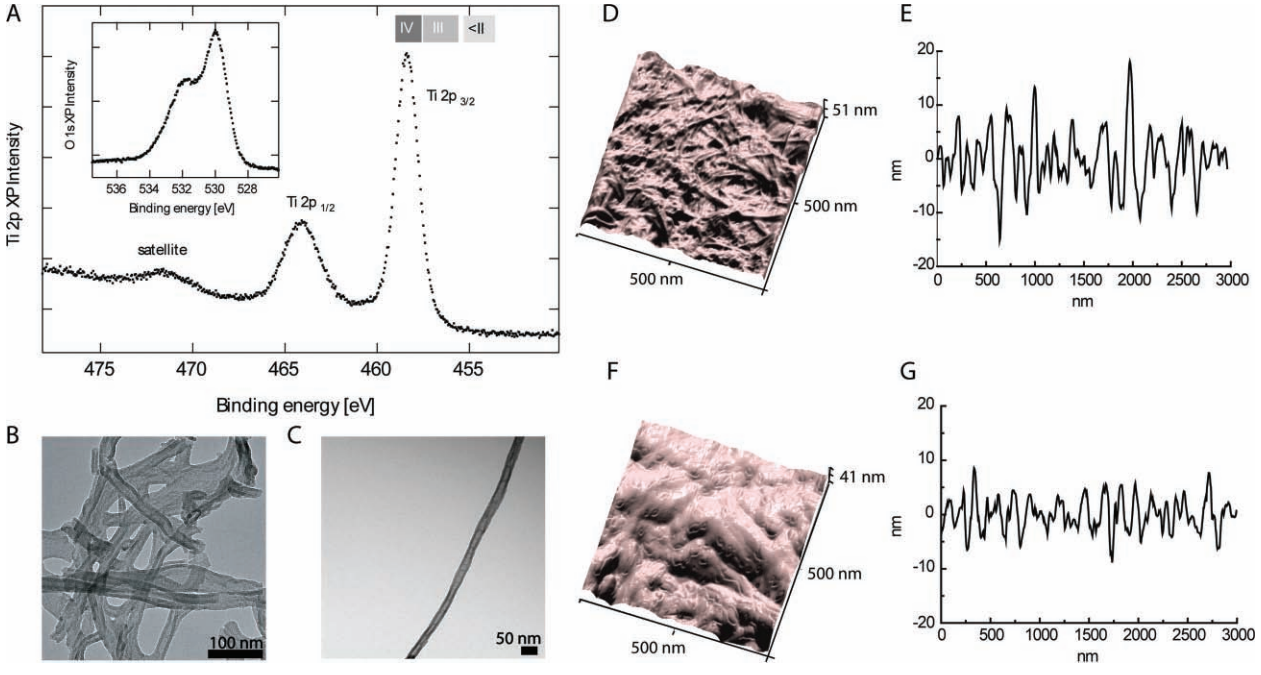

Figure 2. A) Titanium 2p and oxygen 1s (inset) XPS spectra from the TiO_2-coated nanocellulose aerogel sample. B) TEM micrograph of TiO_2-coated nanocellulose aerogel, showing conformal TiO_2 layers with thicknesses of about 7 nm. C) A cellulose nanofibril as selected from the edge of the aerogel to illustrate more clearly the uniformity of the TiO_2 coating. D) An AFM 3D topographical image of the uncoated, drop-cast nanocellulose film, revealing clearly the aggregated nanofibrils. E) A height profile of the film, showing an rms roughness of 5 nm. F) An AFM 3D topographical image of the nanocellulose film after CVD, showing the conformal TiO_2 coating covering the nanofibrils. Smoothed surface due to the TiO_2 is also shown by the height profile (G), with a calculated rms roughness of 3 nm.

surface.[31] In X-ray diffraction (XRD) analysis, no peaks of crystalline TiO_2 could be resolved, suggesting that amorphous material (typical for low-temperature deposition) is deposited or that the crystal sizes are very small. TEM images show that the thickness of the coating is quite uniform (≈7 nm) using the present deposition conditions (Figure 2B,C). The TiO_2 layer acts as a stabilizer for the aerogel, as the coated nanocellulose aerogel was considerably more stable under the electron beam. The total amount of titanium deposited on the aerogel is 8.0–8.6 wt% as determined by inductively coupled plasma – atomic emission spectroscopy. As a reference for the aerogel samples, the same CVD procedure was performed for a 30 μm thick nanocellulose film prepared by drop-casting where the porosity is essentially collapsed and also for a filter paper (see Experimental Section for details). The amount of titanium deposited on the film and filter paper were 0.3 and 0.9 wt%, respectively, which are an order of magnitude less than that deposited on the aerogel, due to the difference in porosity and surface area. Finally, the coverage of the TiO_2 coating on aerogels, filter papers, and films was demonstrated by atomic force microscopy (AFM). First, a representative 3D AFM topographical image of an uncoated, drop-cast nanocellulose film clearly shows nanoscale morphology of the aggregated nanofibrils (Figure 2D). It shows a characteristic surface profile (Figure 2E) with a root mean square (rms) roughness of ≈5 nm. This corresponds well with the previous study of spin-coated nanocellulose films.[33] After CVD, the conformal TiO_2 coating smoothens the surface, and a more uniform height profile is formed (Figure 2F,G). This is also seen as a smaller rms roughness of ≈3 nm.

Previously, macroscopic cellulose fibers, paper sheets, filter papers, and even cellulose nanofibrils have been hydrophobized by various types of surface coatings, for example by "graft-on-graft" and post-functionalization,[34] CVD[35] followed by hydrolyzation and polymerization,[36] a multistep synthesis and layer-by-layer deposition,[37] surface silylation,[38] surface esterification,[39] plasma-enhanced CVD,[40] solution immersion,[41] a multistep solid–gas method, and sol–gel methods.[42] In comparison to the previous methods, the present approach is a particularly simple one-step procedure.

2.3. Photoswitchable Water Absorption in TiO_2-Coated Nanocellulose Aerogels

Next, water absorption into the nanocellulose aerogel was investigated using millimeter-sized bulk specimens cut from bigger samples with a razor blade (see **Table 1**). The untreated nanocellulose aerogel is highly hydrophilic due to the hydroxyl groups on the nanofibril surfaces and the relatively high surface area in relation to nanofibril volume. The amount of water absorbed was measured by immersing an untreated aerogel in water for 30 min, and weighing the aerogel after removal from the water. An untreated nanocellulose aerogel absorbs water ca. 35 times its own weight (absorbent capacity $m_{\text{absorbed water}}/m_{\text{aerogel}} = 35$, **Table 2**). The measured volume increase was below 2%. Such a high absorption value is qualitatively expected, given the aerogel porosity of 98%, and the densities of water and cellulose (1.00 and 1.55 g cm^{-3}, respectively). Therefore, the material can be classified as superabsorbent, even if order-of-magnitude higher absorbent capacities have been reported for carefully optimized superabsorbents. By contrast, upon TiO_2 coating, very little water is absorbed within the aerogel: simple weighing suggests that after forced immersion in a water bath there would be only a maximum of 0.6 times the aerogel weight of water absorbed. However, it should be noted that a large fraction of this water may actually be adsorbed onto the surface due to the adhesive pinning of water in spite of the high hydrophobicity (to be discussed later), and not within the network. Adhesive pinning has been reported even for superhydrophobic surfaces.[43] One can conclude that the TiO_2-coated aerogels are essentially water-repellent, but UV illumination strongly increases the hydrophilicity of TiO_2 due to defect formation in TiO_2 in which the photogenerated oxygen vacancies of TiO_2 are presumably favorable for water adsorption.[15] Therefore, absorption is drastically increased and 16 times of the aerogel weight of water is absorbed. In comparison, the untreated hydrophilic filter paper with a porosity of ≈73% can absorb only 1.4 times its own weight. This suggests that the pore network and structure of the aerogel skeleton at different length scales are essential to achieve a high water-absorbing capacity.

These effects manifest in a profound manner also in the water contact angle measurements. A water droplet applied to an uncoated nanocellulose aerogel surface is absorbed very

Table 2. Water absorption test of different substrates.

Substrate	Absorbent capacity [$m_{water}/m_{substrate}$]
Untreated aerogel	35 ± 2
TiO_2-coated aerogel	0.6 ± 0.3[a)]
UV-illuminated TiO_2-coated aerogel	16 ± 2
Untreated filter paper	1.4 ± 0.3

a)The contribution from water remaining on surface due to the high adhesive force and the small water uptake cannot easily be distinguished. This may strongly influence the value obtained.

Table 1. Characteristics of the substrates.

	Nanocellulose aerogel	Filter paper	Nanocellulose film
Density [g cm^{-3}]	0.03	0.4	1.3
Porosity [%]	98	73	13
BET surface area [m^2 g^{-1}]	20	1.4	-
Ti [%]	8	0.9	0.3

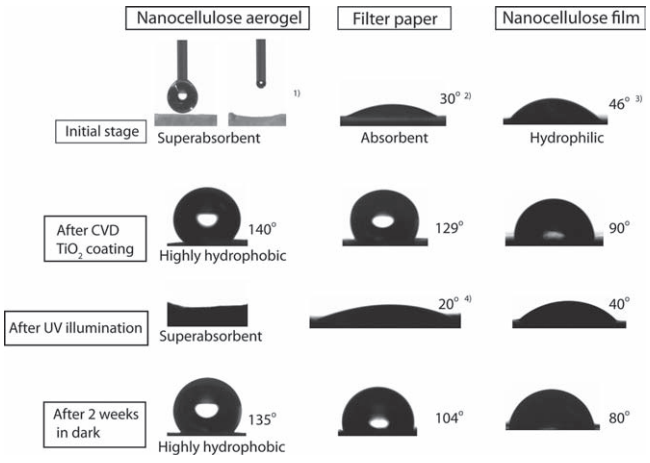

Figure 3. The aqueous absorption and wetting behavior of the nanocellulose aerogel (left), filter paper (center), and nanocellulose film (right) before and after the TiO_2 coating and after UV illumination and storage in the dark. The contact angle values are reported at 1 min unless otherwise stated. 1) The droplet is absorbed within ca. 40 ms. 2) The droplet is absorbed within ca. 1 s. 3) The contact angle value decreases from 49° to 33° over the course of 7.5 min. The value at 1 min is 46°. 4) The droplet is absorbed within 10 s.

quickly (within ca. 40 ms) and therefore the initial nonzero contact angle seems to vanish (**Figure 3**). By contrast, upon TiO_2 deposition, the nanocellulose aerogel becomes highly hydrophobic, with contact angle of 140° (see **Figure 4**). This change is subtle for several reasons. The large change from a strongly absorbing and very hydrophilic material to a near-superhydrophobic and water-repellent material after TiO_2 coating is remarkable considering that, initially, both the substrate and the TiO_2 coatings are fairly hydrophilic. Indeed, the contact angle of water with a smooth TiO_2 surface ranges from 15° to 72° if annealed or stored in the dark.[15,16] Upon UV illumination (see Experimental Section), the TiO_2-coated aerogels underwent a transition from the water-repellent state with a contact angle of 140° back to the water-absorbing state with a vanishing contact angle (Figure 3). The high contact angle and water repulsion slowly recover upon storage in the dark, and after 2 weeks storage the contact angle is 135° (Figure 3). Filter paper (see Experimental Section) is a relevant reference as it has a porous, absorbing structure but is based on large macroscopic cellulose fibers instead of nanofibrils. The uncoated filter paper shows an initial contact angle of ca. 30°, but it decreases rapidly and the droplet becomes absorbed after ca. 1 s. Upon TiO_2 coating, the filter paper becomes hydrophobic and the contact angle increases to ca. 129° (Figure 3). As the water contact angle for a smooth TiO_2 surface can be up to 72°,[15] this proves that in this case the surface topography also plays a role due to the presence of large cellulose fibers. In filter paper, however, appropriate nanoscopic structures are essentially missing and the contact angle becomes smaller than in the case of the nanocellulose aerogel (to be discussed in more detail later). For the drop-cast nanocellulose film, the initial contact angle was 49°, 46° after 1 min, and 33° after 7.5 min. The nanocellulose films also became more hydrophobic upon TiO_2 coating, showing a contact angle ≈90°. Upon UV illumination, the contact angle was reduced to 40°. A slow recovery towards the original contact angles was observed upon storage in the dark (Figure 3).

The structures are discussed next based on SEM and AFM. Figure 4A depicts the structure of the TiO_2-coated aerogel in low magnification, showing a number of sheets due to aggregated nanofibrils as well as fibrous structures, leading to overhang structures and open-pore channels. The aggregates are formed during freeze-drying to prepare the aerogels from the hydrogels. The irregularity in the shape of the sheets and the pores is caused by ice crystallization during the freeze-drying. The sheets can be tens of micrometers in width and slightly bent, leading to a rough surface. At higher magnification, a 3D AFM topographical image (Figure 4B) reveals the internal porous network within the sheets, which has microscale ridges and re-entrant structures (microroughness). At the smallest scale (Figure 4C), the sheets show nanoscale roughness. Consequently, the aerogel consists of different structures and pores at several length scales from microscale to nanoscale, which possibly promotes high water absorption upon UV illumination due to increased capillary effects and the high contact angle of 140° in the water-repellent state. By contrast, the TiO_2-coated filter paper (Figure 4D) consists of macroscopic flattened fibers, which lead to roughness predominantly in the micrometer range, with very little roughness in the nanoscale. The missing nanoscale roughness and porosity leads to a smaller contact angle of 129°. The TiO_2-coated nanocellulose films (Figure 4E) are quite smooth both at the microscale and nanoscale, leading to a smaller contact angle of 90°. The need for

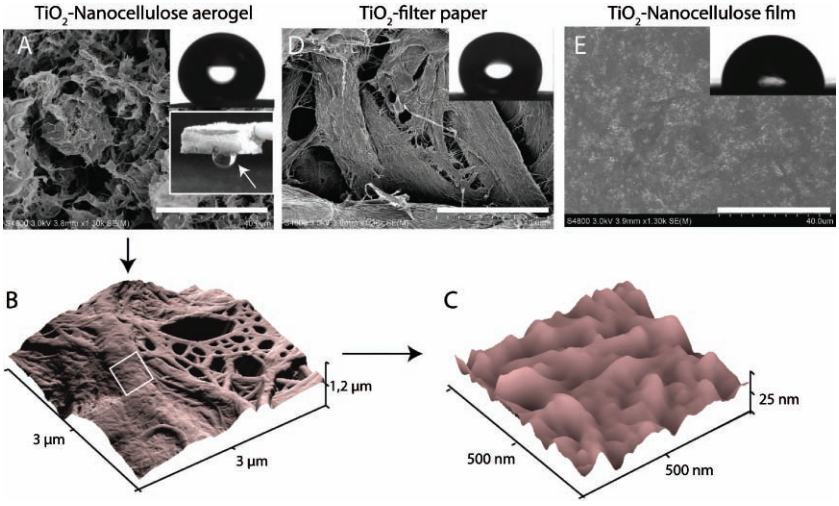

Figure 4. The TiO_2-coated nanocellulose aerogel (A–C) showing pore network and structures at several length scales, leading to a contact angle of ca. 140° and promoting high water absorption under UV illumination. D) TiO_2-coated filter paper with predominantly microscale roughness showing a water contact angle of 129°. E) TiO_2-coated nanocellulose film showing a water contact angle of 90° due to the smooth surface. The scale bar is 40 µm. Inset in A: a water droplet on the TiO_2 nanocellulose aerogel does not roll even if turned upside down, a indicating high adhesive pinning force with water.

structuring at several length scales was also realized in previous (super)hydrophobization studies of cellulose, in which macroscopic cellulose fibers provided the large microscale roughness, but it was necessary to generate a hierarchy, i.e., nanoroughness, by additional means, e.g., by fluorinating nanostructures,[34,37] nanoscale silicone,[36] metal oxide–silane nanocoatings,[42] gold nanoparticles,[44] or by etching the fibers.[40] By contrast, in this study, cellulose nanofibrils are responsible for both micro- and nanoscale roughness due to their spontaneous aggregation, thus allowing particularly simple preparations.

Also, in spite of the high water contact angle of the TiO_2-coated nanocellulose aerogel, the water droplet does not roll off even at large inclinations or when turning the surface upside-down (Figure 4A inset). This phenomenon is known as high-adhesion pinning, and it is explained by the Cassie impregnating wetting regime, where the droplet enters the larger scale grooves of the structure but not the smaller nanostructures.[43]

In conclusion, the TiO_2-coated aerogels show photoswitchable water absorption and wetting phenomena. Even if the absorption and wetting are separate phenomena, being bulk and surface properties, they are still connected. During freeze-drying to prepare the aerogels from the hydrogels, aggregation of the nanofibrils takes place to form pores and structures at different length scales (i.e., a hierarchy). It plays an important role in both absorption and wetting behavior of the TiO_2-coated aerogels. In the superabsorbing state created upon UV illumination, the continuous pore network and structures at different length scales are expected to promote the facile water absorption. On the other hand, in the water-repellent equilibrium state, the structures promote formation of re-entrant structures, evidenced by a high contact angle.

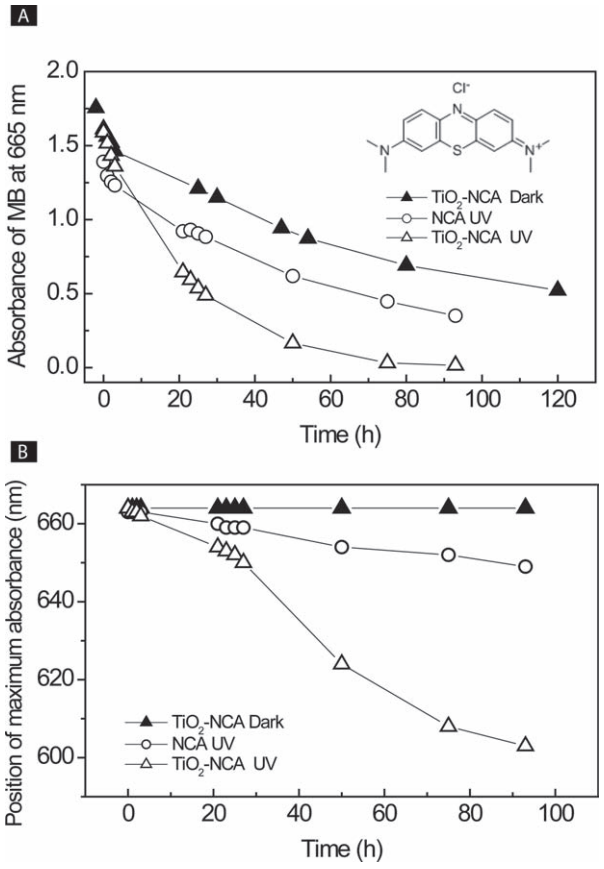

Figure 5. Absorbance of MB (A) and the position of maximum absorbance (B) as a function of time. As a reference for the TiO_2-coated nanocellulose aerogel (NCA) sample illuminated with UV light (open triangles) the absorbance of MB with native nanocellulose aerogel (i.e., no TiO_2 deposition) under UV radiation (open circles) as well as TiO_2-coated nanocellulose aerogel in the dark (filled triangles) are shown. The chemical structure of MB is shown as an inset in (A).

2.4. Photocatalytic Activity

The well known photocatalytic activity of TiO_2—for example, the ability to decompose organic compounds—is based on the oxidation power of photo-induced, active oxygen generated on the TiO_2 surface.[45] Next, the photocatalytic activity of TiO_2-coated nanocellulose aerogels was demonstrated by methylene blue (MB) decomposition.

Figure 5A shows the absorbance of MB at 665 nm as a function of UV illumination time. The absorbance of MB decreased over time in all samples due to adsorption on the fibril surface. However, it can be clearly observed that when both TiO_2 and UV light were present, the absorbance of MB decreased at a significantly higher rate as compared to reference measurements where either the TiO_2 or UV light was absent. The fact that absorbance of MB goes to zero with higher rates indicates that MB is photocatalytically decomposed. Additional spectroscopic evidence for the photodecomposition of MB comes from the position of the maximum absorbance. The main absorbance peak of MB shifted strongly from 665 to 603 nm when both TiO_2 and UV light were present (Figure 5B). This did not take place with reference measurements. The shift results from N-demethylation of MB due to photocatalytic degradation.[46] After 24 h of weak UV illumination, nearly 70% of the MB was decomposed. TiO_2 films deposited at low temperatures are usually amorphous and show quite low or negligible photocatalytic activity, whereas these TiO_2-coated nanocellulose aerogels are photocatalytically active and can be used as a substrate for photocatalysis, e.g., for decomposing organic materials. This tentatively suggests that in fact, some polycrystalline TiO_2 could be deposited, but the crystalline domains are too small to be clearly resolved in XRD, as there is only a 7 nm layer of TiO_2 on top of the very porous nanocellulose substrate.

The photocatalytic phenomena, in combination with the high porosity of the dried nanocellulose aerogels and gel network structure in an aqueous environment, allows new options in applications, e.g., air- and water-purification applications.[47,48]

Previous studies have revealed that the mechanism of photo-induced hydrophilic conversion on TiO_2 is different from the conventional photocatalytic oxidation reaction.[16] Photocatalytic semiconductor oxides such as TiO_2 do not always exhibit photo-induced hydrophilic conversion.[49] The opposite is also true: semiconductors, which display photoinduced hydrophilic conversion, do not always exhibit photo-oxidation capabilities.[49] However, the present TiO_2-coated nanocellulose aerogel exhibits both photo-oxidative decomposition and photo-induced switchable water absorption and wettability.

3. Conclusions

Previously, photoswitchable wetting properties have been demonstrated using TiO_2-coated surfaces.[14] By contrast, in this work, novel photocontrolled switching between the water-superabsorbent and water-repellent states is demonstrated using TiO_2-coated, native nanocellulose aerogel networks. In the stable state, these TiO_2-coated aerogels do not absorb water, evidenced by a high contact angle of 140°. By UV illumination, they become water superabsorbents (absorbing 16 times their own weight), as demonstrated by a vanishing contact angle. The original absorption and wetting properties slowly recover upon storage in the dark. We claim that the nanocellulose aggregations at different length scales, formed during the freeze-drying process used to prepare the aerogels, promote these properties: in the superabsorbent state they promote water absorption due to increased capillary effects, and in the water-repellent state they promote high contact angles due to re-entrant structures, potentially stabilizing air pockets. In addition to photo-induced absorption and wetting behavior, the TiO_2-coated nanocellulose aerogels show also photocatalytic activity, being able to decompose an organic material (methylene blue). Photoswitchable water absorption suggests, for example, microfluidic applications. In addition, the photocatalytic phenomena in combination with the high porosity of the dried nanocellulose aerogels and gel network structure in aqueous environments allow new options such as air- and water-purification applications.

4. Experimental Section

Preparation of the Aqueous Gel of Cellulose I Nanofibrils: The aqueous gels of long and entangled native cellulose I nanofibrils (nanoscopic microfibrillated cellulose) were prepared at Innventia AB (Sweden) using the method described previously.[12]

Preparation of Nanocellulose Aerogels by Vacuum Freeze-Drying: The room temperature 2% (w/w) aqueous gel was placed into a vacuum oven in a silicone mold with a thickness of 3 mm. The temperature of the gel was lowered by the pumping action and the gel froze quickly, and thereafter water sublimed from the frozen sample. The drying was finished when the pressure in the oven remained stable at ca. 10^{-2} mbar. The preparation method, morphology and the properties of the aerogels are described in detail elsewhere.[2] The BET surface area of dried nanocellulose aerogels with thicknesses of 3 mm were ≈20 $m^2\ g^{-1}$ as measured with a Flowsorp II 2300 (Micromeritics) and Coulter Omnisorp 100CX at the temperature of liquid nitrogen (i.e., −196 °C). Before measuring the nitrogen adsorption, the samples were dried at a temperature of 100 °C until a vacuum of 10^{-5} Torr was reached. Both adsorption and desorption isotherms were measured and the surface area was calculated from the adsorption data by using the BET method. (Note: 1 bar = 100 000 Pa ≈ 750 Torr).

Filter Papers: Schleicher & Schuell 589/2 filter paper with a thickness of ≈190 µm, a BET surface area of ≈1.4 $m^2\ g^{-1}$, and a porosity of ≈73% were used as a reference for TiO_2 coating. Porosity was calculated as $\phi = 1 - (\rho_{\text{filter paper}}/\rho_{\text{cellulose fiber}})$, where the density ($\rho$) of filter paper is 0.4 g cm^{-3} and the density of cellulose fiber is 1.5 g cm^{-3}.

Preparation of Nanocellulose Films: Self-supporting, robust, 30 µm thick nanocellulose films were prepared by film-casting from 1% (w/w) aqueous nanocellulose gel. The gel was poured into a Teflon mold and placed into an oven at 30 °C to dry. The density and porosity of the films were 1.3 g cm^{-1} and 13%, respectively.

Chemical Vapor Deposition: The nanocellulose aerogels (25–30 mg) were coated with titanium dioxide (TiO_2) in an atomic layer deposition reactor (F-120, Microchemistry Ltd., Finland). In the CVD process, samples were preheated to 190 °C for 1.5 h and then reacted with the precursor titanium isopropoxide, $Ti(C_3H_7O)_4$, (0.7 g, Sigma-Aldrich, 99.999%) at 190 °C and 1–5 kPa for 2 h by vaporizing the precursor at 40 °C and carrying it through the sample with nitrogen (AGA, 99.999%). In the end, the sample was purged with nitrogen at the reaction temperature for 2 h to remove any unreacted species, and then cooled in nitrogen flow to room temperature for unloading. After the reaction, the coated nanocellulose aerogel was exposed to air. The same CVD procedure was performed for filter papers and nanocellulose films, using 0.7 and 0.3 g of the precursor, respectively. In each sample, the mass of the precursor depended on the mass of the cellulose substrate (the same ratio was maintained).

Characterization: After deposition, the titanium content of the nanocellulose aerogels, filter papers and films was analyzed with inductively coupled plasma – atomic emission spectroscopy (Varian Liberty ICP-AES). X-ray photoelectron spectroscopy (SSX-100 ESCA spectrometer) was used to study the composition of the surface of the sample after deposition. The C 1 s peak of adventitious carbon at 285 eV was used as a binding energy reference. The FE-SEM images were acquired with a Hitachi S-4800 field-emission scanning electron microscope. Prior to imaging, the samples were coated with 5 nm of Pt/Pd using a Cressington 208HR Sputter Coater. A JEOL JEM-3200 FSC (Jeol Ltd., Japan) microscope was used for the cryogenic-TEM imaging to characterize the morphology of the nanocellulose dispersions. The sample preparation is described in detail elsewhere.[2] Bright-field TEM (FEI Tecnai 12) was used to study the structure of titanium-dioxide-coated aerogel. Small pieces of sample were broken off using tweezers and were placed in an oyster-type copper grid (300/100 mesh). Parts of the edges of the broken pieces were sufficiently thin to allow studies by TEM. The transmission electron microscope was operated at an accelerating voltage of 120 kV. TEM could not be used for pure nanocellulose aerogel samples because the beam destroys the cellulose. AFM characterizations were performed on a Veeco Dimension 5000 Scanning Probe Microscope with a Nanoscope V controller (Digital Instruments, Inc.). All samples (uncoated and coated aerogels, filter papers, and films) were robust bulk samples and were measured without treatment. Al-coated silicon AFM tips (NSC 15/AIBS, MikroMasch, Estonia) with a tip radius of 10 nm were used to probe the surface profiles of uncoated and coated aerogels, filter papers, and films. Tapping-mode AFM imaging was used according to well-established procedures. Scanning was conducted for scale sizes ranging from 500 nm to 3 µm across with scanning rates of 0.8–1 Hz under variable loading conditions (hard- and light-tapping modes). All images were post-treated with Gwyddion 2.19 Software (http://gwyddion.net). To highlight only the smallest features on the surface, sixth-order polynomial background correction was performed to remove the large-scale unevenness of the robust self-supporting "bulk" samples in Figure 2D,F and 4C. Also, the root mean square roughness was evaluated from the profiles.

Wetting Properties of Cellulose Materials: A CAM 200 Optical Contact Angle Meter (KSV Instruments) was used to study the wetting behavior of the cellulose surfaces. Static water contact angle (CA) measurements were conducted over time to investigate the absorption ability, spreading behavior and stability of the surface. All the CA values were reported at 1 min, except those of filter paper and UV-illuminated, TiO_2-coated filter paper, which absorbed the drop within 10 s. Note that the contact angle values of hydrophilic, native nanocellulose film and UV-illuminated, TiO_2-coated nanocellulose film decrease smoothly as a function of time. The contact angle value calculations are based on the Young–Laplace equation. For nanocellulose films, images of a deposited droplet were recorded for every 10–30 s, and the CA was calculated. For the native nanocellulose aerogels and filter papers, as well as UV-illuminated samples, the fast mode, where images were recorded every 40 ms, was used. Drop size varied from 2–6 µL depending on the measured area and sample. 5–8 reference samples were measured, with a typical deviation of ±3°.

Water Absorption Test: Aerogels were weighed and immersed under the water for 30 min. The TiO_2-coated aerogels are water repellent and they were forced to sink, otherwise they would float on the water, while

uncoated and UV-illuminated, TiO_2-coated aerogels became wetted immediately. The sample was removed from the water bath and weighed. The amount of absorbed water was calculated from the masses (m) as Absorbed Amount = $(m_{\text{wet aerogel}} - m_{\text{dry aerogel}})/m_{\text{dry aerogel}}$.

UV Light Illumination: Samples were illuminated under ambient conditions in quartz cuvettes for different time periods (10, 30, and 60 min) using a Rayonet photochemical reactor (Southern New England Ultraviolet Co., Middletown, CT, USA) equipped with 16 RPR-3500 Å lamps (intensity approximately 9.2 mW cm^{-2}, $\lambda = 350$ nm).

Photocatalytic Activity: Photocatalytic degradation measurements were performed using MB as a probe molecule. The reaction was carried out in a quartz cell containing 3 mL of 0.03 mM aqueous MB solution and 3 mg of TiO_2-coated nanocellulose aerogel. UV illumination was performed through the windows of the cell with two Sylvania Blacklight Blue UV lamps (peak maximum at 365 nm, intensity ≈2 mW cm^{-2}). The concentration of MB in the solution was followed by UV–vis spectroscopy. Measurements with coated aerogel in the absence of UV light and pure nanocellulose aerogel under UV light were performed as references.

Acknowledgements

The authors acknowledge Prof. Markku Leskelä, Dr. Harri Kosonen, Prof. Outi Krause, Heli Vuori, Dr. Jouko Lahtinen, Dr. Riikka Puurunen, Prof. Lars Berglund, Prof. Lars Wågberg, Prof. Gero Decher, Prof. Janne Laine, and Dr. Marina Lindblad for collaboration and discussions. AFM images were obtained in the Nanomicroscopy Center at Aalto University. Antti J. Soininen is acknowledged for expertise in AFM analysis. This work has been mainly performed as a part of the "Nanostructured Cellulose Products" project in the Finnish-Swedish Wood Material Science Research Program and partly in SustainComp. Financial support from Academy of Finland and the Finnish Funding Agency for Technology and Innovation (TEKES) is acknowledged.

Received: July 15, 2010
Revised: August 19, 2010
Published online: December 6, 2010

[1] A. C. Pierre, G. M. Pajonk, *Chem. Rev.* **2002**, *102*, 4243.
[2] M. Pääkkö, J. Vapaavuori, R. Silvennoinen, H. Kosonen, M. Ankerfors, T. Lindström, L. A. Berglund, O. Ikkala, *Soft Matter* **2008**, *4*, 2492.
[3] R. T. Olsson, M. A. S. Azizi Samir, G. Salazar Alvarez, L. Belova, V. Ström, L. A. Berglund, O. Ikkala, J. Nogués, U. W. Gedde, *Nat. Nanotechnol.* **2010**, *5*, 584.
[4] S. J. Eichhorn, A. Dufresne, M. Aranguren, N. E. Marcovich, J. R. Capadona, S. J. Rowan, C. Weder, W. Thielemans, M. Roman, S. Renneckar, W. Gindl, S. Veigel, J. Keckes, H. Yano, K. Abe, M. Nogi, A. N. Nakagaito, A. Mangalam, J. Simonsen, A. S. Benight, A. Bismarck, L. A. Berglund, T. Peijs, *J. Mater. Sci.* **2010**, *45*, 1.
[5] S. Iwamoto, W. Kai, A. Isogai, T. Iwata, *Biomacromolecules* **2009**, *10*, 2571.
[6] P. Langan, Y. Nishiyama, H. Chanzy, *Biomacromolecules* **2001**, *2*, 410.
[7] H. Jin, Y. Nishiyama, M. Wada, S. Kuga, *Colloid Surf.—A* **2004**, *240*, 63.
[8] R. Gavillon, T. Budtova, *Biomacromolecules* **2008**, *9*, 269.
[9] A. F. Turbak, F. W. Snyder, K. R. Sandberg, *J. Appl. Polym. Sci.—Appl. Polym. Symp.* **1983**, *37*, 815.
[10] K. Abe, S. Iwamoto, H. Yano, *Biomacromolecules* **2007**, *8*, 3276.
[11] T. Saito, S. Kimura, Y. Nishiyama, A. Isogai, *Biomacromolecules* **2007**, *8*, 2485.
[12] M. Pääkkö, M. Ankerfors, H. Kosonen, A. Nykänen, S. Ahola, M. Österberg, J. Ruokolainen, J. Laine, P. T. Larsson, O. Ikkala, T. Lindström, *Biomacromolecules* **2007**, *8*, 1934.
[13] M. Henriksson, G. Henriksson, L. A. Berglund, T. Lindström, *Eur. Polym. J.* **2007**, *43*, 3434.
[14] B. Xin, J. Hao, *Chem. Soc. Rev.* **2010**, *39*, 769.
[15] R. Wang, K. Hashimoto, A. Fujishima, M. Chikuni, E. Kojima, A. Kitamura, M. Shimohigoshi, T. Watanabe, *Nature* **1997**, *388*, 431.
[16] R. Wang, K. Hashimoto, A. Fujishima, M. Chikuni, E. Kojima, A. Kitamura, M. Shimohigoshi, T. Watanabe, *Adv. Mater.* **1998**, *10*, 135.
[17] X. Feng, J. Zhai, L. Jiang, *Angew. Chem. Int. Ed.* **2005**, *44*, 5115.
[18] J. Malm, E. Sahramo, M. Karppinen, R. H. A. Ras, *Chem. Mater.* **2010**, *22*, 3349.
[19] A. Dong, Y. Wang, Y. Tang, N. Ren, Y. Zhang, Y. Yue, Z. Gao, *Adv. Mater.* **2002**, *14*.
[20] Y. Shin, J. Liu, J. H. Chang, Z. Nie, G. J. Exarhos, *Adv. Mater.* **2001**, *13*, 728.
[21] J. Huang, T. Kunitake, *J. Am. Chem. Soc.* **2003**, *125*, 11834.
[22] B. Sun, T. Fan, J. Xu, D. Zhang, *Mater. Lett.* **2005**, *59*, 2325.
[23] J. Huang, T. Kunitake, S.-Y. Onoue, *Chem. Commun.* **2004**, 1008.
[24] M. Kemell, V. Pore, M. Ritala, M. Leskelä, M. Lindén, *J. Am. Chem. Soc.* **2005**, *127*, 14179.
[25] T. H. Han, J. K. Oh, J. S. Park, S.-H. Kwon, S.-W. Kim, S. O. Kim, *J. Mater. Chem.* **2009**, *19*, 3512.
[26] *Absorbent Polymer Technology Volume 8: Studies in Polymer Science* (Eds: L. Brannon-Peppas, R. S. Harland), Elsevier, Amsterdam, **1990**, 67–102.
[27] *Modern Superabsorbent Polymer Technology* (Eds: F. L. Buchholz, A. T. Graham), Wiley-VCH, New York **1998**.
[28] *Biorelated Polymers and Gels* (Ed: T. Okano), Academic Press, Boston **1998**.
[29] K. L. Siefering, G. L. Griffin, *J. Electrochem. Soc.* **1990**, *137*, 814.
[30] J. Keränen, E. Iiskola, C. Guimon, A. Auroux, L. Niinistö, *Stud. Surf. Sci. Catal.* **2002**, *143*, 777.
[31] L. Q. Wang, D. R. Baer, M. H. Engelhard, A. N. Schultz, *Surf. Sci.* **1995**, *344*, 237.
[32] R. Wang, N. Sakai, A. Fujishima, T. Watanabe, K. Hashimoto, *J. Phys. Chem. B* **1997**, *103*, 2188.
[33] C. Aulin, S. Ahola, P. Josefsson, T. Nishino, Y. Hirose, M. Österberg, L. Wågberg, *Langmuir* **2009**, *25*, 7675.
[34] D. Nyström, J. Lindqvist, E. Östmark, A. Hult, E. Malmström, *Chem. Commun.* **2006**, 3594.
[35] C. Aulin, J. Netrval, L. Wågberg, T. Lindström, *Soft Matter* **2010**, *6*, 3298.
[36] S. Li, H. Xie, S. Zhang, X. Wang, *Chem. Commun.* **2007**, 4857.
[37] G. Goncalves, P. A. A. P. Marques, T. Trindade, C. P. Neto, A. Gandini, *J. Colloid Interface Sci.* **2008**, *324*, 42.
[38] M. Andresen, S.-L. Johansson, B. S. Tanem, P. Stenius, *Cellulose* **2006**, *13*, 665.
[39] A. G. Cunha, C. Freire, A. Silvestre, C. P. Neto, A. Gandini, E. Orblin, P. Fardim, *Biomacromolecules* **2007**, *8*, 1347.
[40] B. Balu, V. Breedveld, D. W. Hess, *Langmuir* **2008**, *24*, 4785.
[41] S. Li, S. Zhang, X. Wang, *Langmuir* **2008**, *24*, 5585.
[42] Y. H. Li, S. Wei, *J. Chem. Lett.* **2010**, *39*, 20.
[43] M. J. Liu, Y. M. Zheng, J. Zhai, L. Jiang, *Acc. Chem. Res.* **2010**, *43*, 368.
[44] T. Wang, X. Hu, S. Dong, *Chem. Commun.* **2007**, 1849.
[45] Y. Ohko, K. Hashimoto, A. Fujishima, *J. Phys. Chem. A* **1997**, *101*, 8057.
[46] T. Zhang, T. Oyama, A. Aoshima, H. Hidaka, J. Zhao, N. Serpone, *J. Photochem. Photobiol. A* **2001**, *140*, 163.
[47] H. Bai, Z. Liu, D. D. Sun, *Chem. Commun.* **2010**, *46*, 6542.
[48] M. R. Hoffmann, S. T. Martin, W. Choi, D. W. Bahnemann, *Chem. Rev.* **1995**, *95*, 69.
[49] T. Watanabe, S. Fukayama, M. Miyauchi, A. Fujishima, K. Hashimoto, *J. Sol–Gel Sci. Technol.* **2000**, *19*, 71.